applied sciences

MDPI

Article

Detection of Broken Bars in Induction Motors Using Histogram Analysis of Current Signals

Veronica Hernandez-Ramirez [1,2], Dora-Luz Almanza-Ojeda [1], Juan-Jose Cardenas-Cornejo [1], Jose-Luis Contreras-Hernandez [1] and Mario-Alberto Ibarra-Manzano [1,*]

[1] Electronics Engineering Department, Engineering Division of the Irapuato-Salamanca Campus, University of Guanajuato, Carr. Salamanca-Valle de Santiago KM. 3.5 + 1.8 Km., Salamanca 36885, Mexico; v.hernandez.ramirez@ugto.mx (V.H.-R.); dora.almanza@ugto.mx (D.-L.A.-O.); jj.cardenascornejo@ugto.mx (J.-J.C.-C.); jose.contreras@ugto.mx (J.-L.C.-H.)

[2] Multidisciplinary Studies Department, Engineering Division of the Irapuato-Salamanca Campus, University of Guanajuato, Av. Universidad, Yuriria 38944, Mexico

* Correspondence: ibarram@ugto.mx

Abstract: The lifetime of induction motors can be significantly extended by installing diagnostic systems for monitoring their operating conditions. In particular, detecting broken bar failures in motors is important for avoiding the risk of short circuits or other accidents with serious consequences. In the literature, many approaches have been proposed for motor fault detection; however, additional generalized methods based on local and statistical analysis could provide a low-complexity and feasible solution in this field of research. The proposed work presents a methodology for detecting one or two broken rotor bars using the sums and differences histograms (SDH) and machine learning classifiers in this context. From the SDH computed in one phase of the motor's current, nine texture features are calculated for different displacements. Then, all features are used to train two classifiers and to find the best displacements for faults and health identification in the induction motors. A final experimental evaluation considering the best displacements shows an accuracy of 98.16% for the homogeneity feature and a few signal samples used in a decision tree classifier. Additionally, a polynomial regression curve validates the use of 50 samples to obtain an accuracy of 88.15%, whereas the highest performance is achieved for 250 samples.

Keywords: broken rotor bars; SDH; current signals; induction motors; texture features; regression analysis

Citation: Hernandez-Ramirez, V.; Almanza-Ojeda, D.-L.; Cardenas-Cornejo, J.-J.; Contreras-Hernandez, J.-L.; Ibarra-Manzano, M.-A. Detection of Broken Bars in Induction Motors Using Histogram Analysis of Current Signals. *Appl. Sci.* **2023**, *13*, 8344. https://doi.org/10.3390/app13148344

Academic Editors: Xiaojian Yi and Xingxing Jiang

Received: 20 June 2023
Revised: 14 July 2023
Accepted: 17 July 2023
Published: 19 July 2023

1. Introduction

Induction motors are electro-mechanical elements of the industry used essentially for manufacturing, power generation, and transportation [1]. Due to the critical role of the induction motor in various sectors, detecting faults has become a vast field of research in recent years [2]. As an electromechanical machine, induction motor faults are categorized as electrical or mechanical. Approximately 45–55% of mechanical failures are typically located in the components most exposed to damages, such as the stator, the rotor, and the bearings. Similarly, electrical faults are mainly associated with stator winding faults, broken rotor bar (BRB) faults, phase unbalance, and single phasing faults [1]. Analyzing vibration, voltage, and current signals has been widely used for monitoring motor faults. In general, the success of defect classification depends on the correct choice of the signal and its acquisition techniques that better provide information about the motor state [2]. To this aim, current signal acquisition methods have been non-invasive and reliable, contrary to other invasive sensors requiring an instrumentation stage. Additionally, most of the traditional signal processing techniques are used in the time, frequency, and time-frequency domains; the choice of the domain depends on the information required to perform motor fault classification [1].

Some methods in the time domain are MUSIC [3], PCA and LDA [4], quaternions [5], statistics [6], and machine learning based [7,8]. These methods provide low computational cost and quickness in processing. Likewise, domain transformation methods are developed to classify faults as MCSA [9], FFT [10], Wavelet [11], and Hilbert transform [12]. Multiple faults such as stator winding, ball element, outer race, unbalanced, and bearing are diagnosed using the aforementioned methods. The broken rotor bar (BRB) detection is one of the most analyzed faults due to its severity and for avoiding subsequent major failures [13]. In this context, some works in the literature propose the diagnosis and classification of BRB in the time domain using machine learning methods and achieving accurate classification results. In [14], stator current signals in the time domain are used to classify four cases of BRB and healthy motor case using support vector machine (SVM), k-nearest neighbor (KNN), fuzzy ARTMAP, and multilayer perceptron network, showing an accuracy of 95%.

In the spatial domain context, histograms are graphical objects in statistics that estimate any density function. They are used to analyze quantitative data and extract features that describe local behaviors [15]. Previous work proposed in [16] uses statistical histograms to identify and classify failures. The histograms detect healthy and unhealthy bearings through infrared thermal images. Moreover, in [17], five image segmentation methods were applied to extract statistical information from thermal images and use histograms to determine different bearing fault conditions. Similarly, [18] proposed the classification of broken rotor bars, bearing faults, and misalignment analyzing the segmentation of gray-scale infrared imaging. The histogram obtains the image asymmetry, calculating first-order statistical features in the time domain.

In the case of frequency analysis, discrete wavelet transform (DWT) is a method presented in related works for motor fault detection [2]. This case was presented in [19], where features are extracted from the acoustic sign through DWT, statistical histograms, and local binary patterns (LBP). SVM and KNN classification algorithms were applied, obtaining an accuracy of 99.8% in detecting healthy motor, one, two, and three BRB and bearing defects. Moreover, fast Fourier transform (FFT)-based algorithms were proposed to calculate two current spectrograms based on multiple short-time Fourier transforms (STFT). A segmentation task is also performed through the Otsu algorithm [20]. After, a histogram is calculated to highlight its non-stationary frequencies, aiming to obtain the kurtosis. It is used to classify half, one, two BRBs, and healthy conditions with a normal distribution with 100% efficiency. A histogram of oriented gradients (HOG) is an essential approach to fault detection. In [21], three stator currents were transformed into three images, and the HOG was used to extract interesting features of a healthy state, bearing faults, BRB faults, short-circuit faults, and their combinations. A multi-layer artificial neural network (ANN) was trained to classify, achieving 95% accuracy. Similarly, in [22], the stator current was used to extract intensity gradients and edge directions to classify healthy motor and one to four BRB faults in the time domain. The features were calculated through HOG and used to train an ANN, obtaining an accuracy of 96%.

It is noticeable that the scientific community has increased its interest in induction motor fault monitoring due to its essential role in the industry. The choice of motor diagnosis through the analysis of current in the time allows for the design of feasible and cheap sensors to acquire the signal of the motor. In this context, this article proposes a low-complexity and statistical approach to identify the operating condition of induction motors by evaluating texture features based on SDHs. The current from the induction motor is used to calculate the SDH and the nine texture attributes evaluating two different sets of displacements, called Δ. Both displacement sets are used to train and test the decision tree classifier. The classifier is trained to detect one and two BRB and health conditions to find the best displacements that perform best. Based on the classification results, the best Δ displacements are used to train and test two more classifiers: the bagged decision tree and the K-nearest neighbor KNN. From this, the texture feature with the highest performance is finally chosen. A polynomial regression curve shows the best trade-off between samples and performance.

The rest of the paper is organized in the following order. Section 2 presents the methodology based on histograms of sums and differences and deeply analyses the displacements for texture calculation. Then, three conducted experimental tests of the classification results obtained and a comparison with related works are described in Section 3. Lastly, the discussion and conclusions are presented in Section 4.

2. Proposed Methodology

Broken bar fault detection is one of the most challenging conditions in an induction motor because the motor continues working without notable malfunctions. However, one motor bar's damage extends the fault condition to the attached bars, consequently increasing energy consumption. The presence of a broken bar can be detected in the current signal. Therefore, the increased current demand represents multiple broken bars facilitating the diagnosis.

Figure 1 shows a global description of the proposed method for detecting one broken rotor bar (1BRB), two broken rotor bars (2BRB), and health in induction motors. An instrumented test bench allows the acquisition of one phase's current signal represented by $S(n)$ to gather the database used in the experimental tests. Several electronic components allow the signal acquisition and conditioning of the motor current signal. The sum histogram h_s and difference histogram h_d are computed for a predefined window size Ws. Then, the texture feature module extracts nine features from h_s and h_d histograms considering different displacements for the sliding window, defined as Δ. Considering different displacements and their combinations, one vector is stored for each texture feature and displacement. The fault classifier module performs three tests, Test A, Test B, and Test C. During Test A and Test B, all texture features are considered, and different Δ values are predefined. The displacements used for each test are defined in Section 2.3. The best classification resulting from Test A and B is used to train a decision tree classifier in Test C for all texture features. Then, Test C allows selection of the texture feature with the highest performance. After that, the chosen selected feature is used to train two more classifiers: a bagged decision tree and a k-nearest neighbor (KNN) classifier.

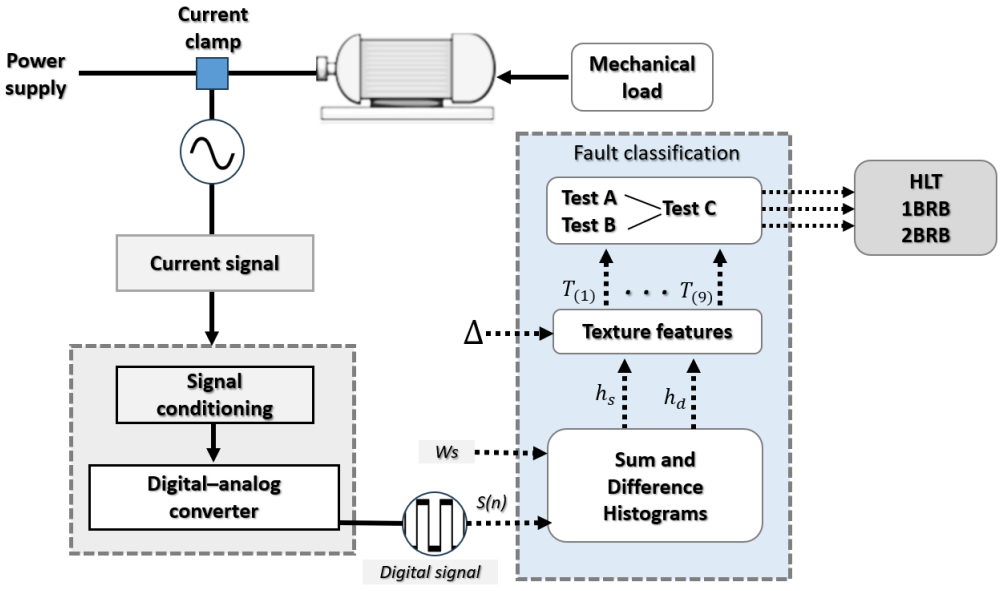

Figure 1. Proposed methodology for HLT, 1BRB, and 2BRB fault classification.

2.1. Experimental Test Bench

An induction motor is an electromagnetic machine with intertwined electrical and magnetic circuits that converts the electrical current through the stator windings into mechanical energy. This energy is produced due to the flux of current where a rotating magnetic field is produced [23]. The presence of broken bars produces a disturbance in

the rotor's magnetic field, intensifying torque modulation and vibrations within the motor. The sidebars also suffer a progressive deterioration due to the tension generated by motor bar fractures [24]. Thus, the effect of broken rotor bars can be detected through the current signals emitted by the motor power supply or by vibrational signals. Some approaches for motor fault detection consider both kinds of signals. In this work, only one current phase is processed and analyzed for detecting the motor's 1BRB, 2BRB, or HLT condition.

Figure 2 shows the test bench used to acquire the current signals for validating the proposed methodology. The acquisition module uses a WEG 00136APE48T two poles three-phase induction motor of 1 hp, 28 bars, and 220 V AC power supply at 60 Hz. Motor initiation is controlled by a relay that synchronizes data acquisition with the ignition switch. The data acquisition module (DAS) uses a phase of the current signal acquired by a Fluke Model i200s AC clamp with a 16-bit analog-to-digital converter (ADS7809) from Texas Instruments Incorporated. The instrumentation system provides a sample rate of 1.5 kHz.

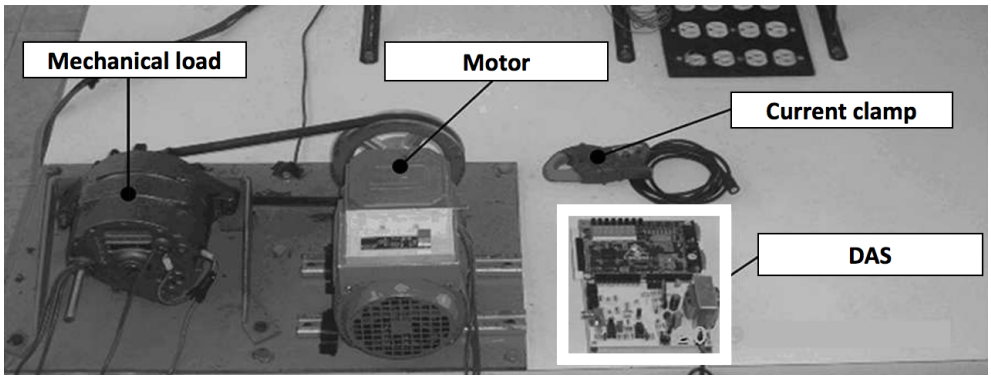

Figure 2. Data acquisition module.

Broken rotor bars effects are observed in the current signal acquired $S(n)$ through the harmonics that alter the uniformity. Therefore, the current signal can be statistically analyzed to detect broken bars anomalies. Sampled signals are below the tenth harmonic, allowing variations detection within the signal. Thirty signals were acquired in one of the motor phases for each fault and health state with 4096 samples. Based on the plots shown in Figure 3, the amplitude of the signal increases for fewer samples in 2BRB like shows in Figure 3c than for the rest of the cases. This increment results from a greater demand for current to the power system. The amplitude variation of the current signal allows statistical analysis for detecting unusual patterns in the motor state. The acquired signal is conditioned by analog-to-digital (A/D) conversion, corresponding to the 16-bit format in the DAS. A bank of 90 tests was obtained for signal conditioning, 30 for each motor state (HLT, 1BRB, 2BRB). The broken bars in the motor were artificially produced by making circular holes of 7.938 mm diameter to cause partial fractures of the bar illustrated in Figure 4. The rotor part is shown for extracting the HLT, 1BRB, and 2BRB samples.

2.2. Sum and Difference Histograms for Texture Classification

A histogram shows the distribution of a numerical variable contained in a dataset that measures the frequency of values within the analyzed vector. Similarly, the sum and difference histograms (SDH) method represents the frequency of values considering the addition or subtraction between a reference point R_s in the dataset and its neighborhood. In this work, the histograms represent the discrete joint probability functions locally calculated using only one phase of the current signal $S(n)$ acquired from an induction motor. The SDHs are computed in a small analysis window denoted as W_s, which counts the frequency values inside. The W_s window is depicted in red in Figure 5 for illustrating the range of the local data around each R_s point in the current vector $S(n)$.

The size of W_s helps to find the best precision by varying distances around R_s. The histograms are calculated in $S(n)$ over the W_s windows centered at R_s, and it is displaced

along the vector according to the set of values in Δ. Different displacements are considered to more accurately assess the local behavior of current for the BRB faults. The Δ values with the best performance were used to evaluate the texture features.

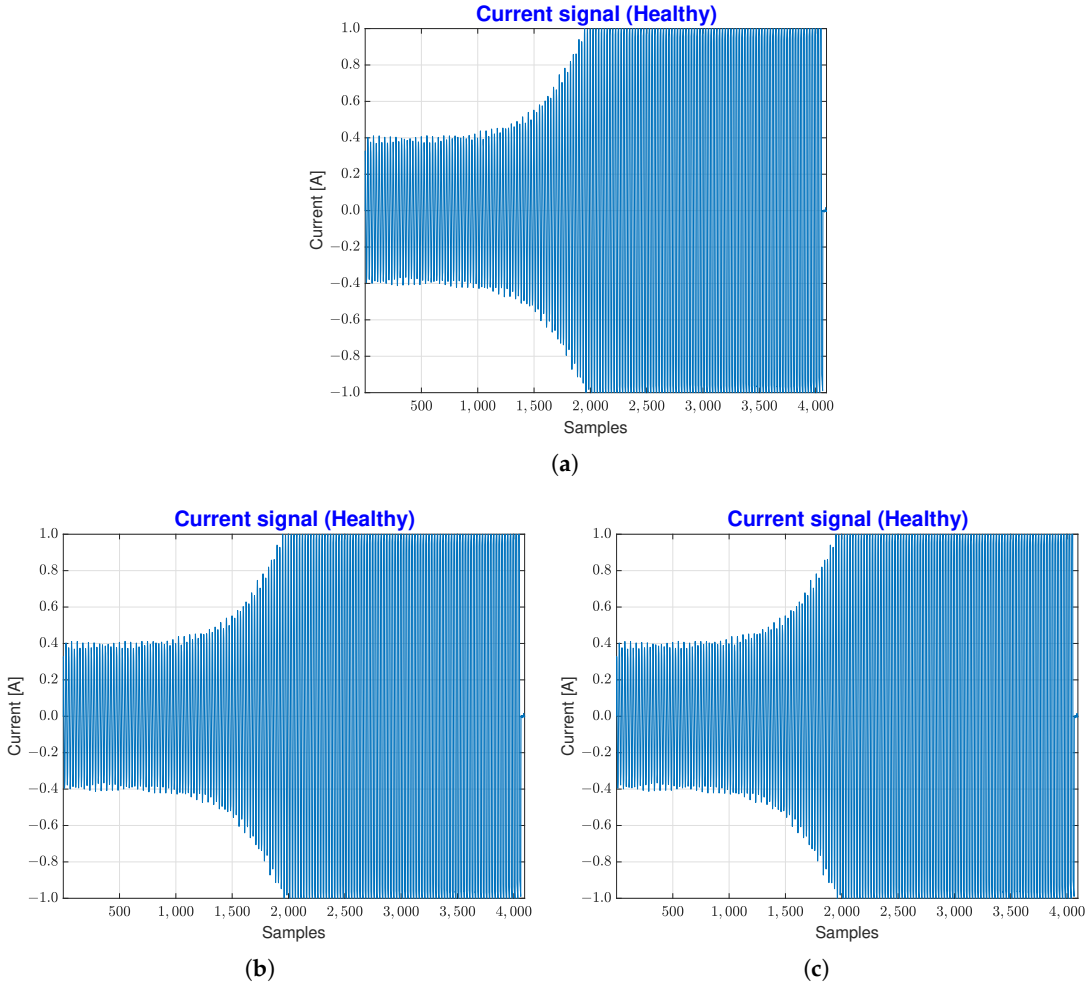

(**a**) (**b**) (**c**)

Figure 3. Single -phase current signals of an induction motor for (**a**) HLT, (**b**) 1BRB, (**c**) 2BRB.

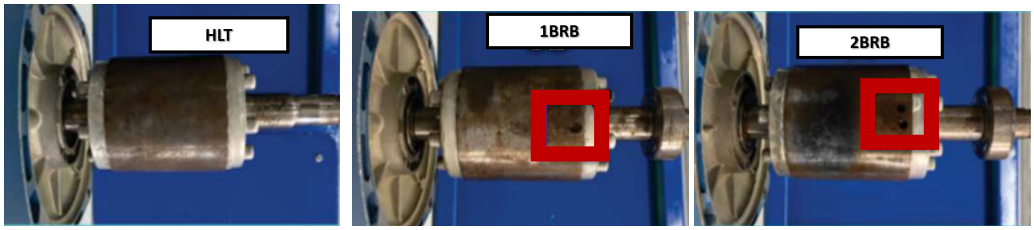

(**a**) (**b**) (**c**)

Figure 4. Squirrel cage rotor images: (**a**) healthy motor, (**b**) 1BRB, (**c**) 2BRB.

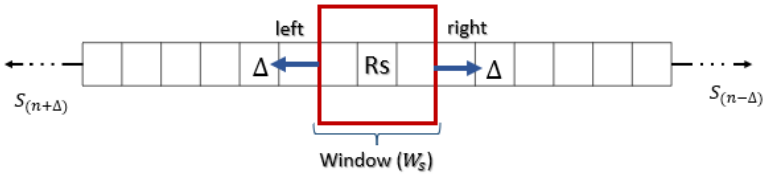

Figure 5. Representation of the sliding window used to calculate the SDH in the signal $S(n)$ using Δ displacements. The displacements to the right compute h_s and to the left, h_d.

The direction of displacements in Δ depends on the histogram to be calculated. Then, the displacements will be applied to the right to calculate the histogram of sums h_s and to the left for the histograms of differences h_d, as illustrated in Figure 6. Based on the Δ displacements, various histograms are computed according to the amplitude of the current signal defined as A_c. The processing will be repeated until the entire vector signal $S(n)$ is scanned.

The SDH establishes a relation between two points in the current signal amplitude separated by a distance (Δ). Then, these points are added or subtracted to obtain the histograms h_s and h_d, respectively, as defined in Equation (1). Let S be a current signal of size N, and each element $n \in [0, N-1]$ represents a signal amplitude defined at displacement Δ. The h_s and h_d histograms are defined in Equation (1).

$$h_s = S(n) + S(n+\Delta) \qquad h_d = S(n) - S(n+\Delta) \tag{1}$$

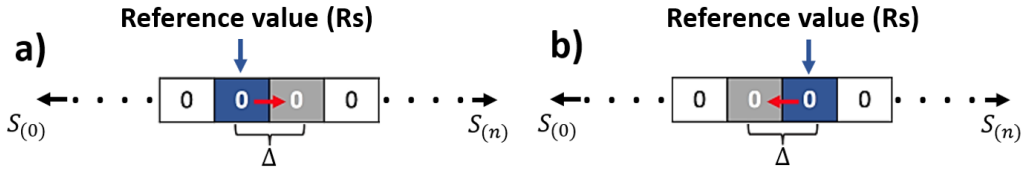

Figure 6. Representation of displacements in S. (**a**) For h_s, its right neighbor value is added, (**b**) h_d is subtracted from its left neighbor value.

The domains of h_s and h_d are $G_s = 2, ..., 2A_c$ and $G_d = -A_c + 1, ..., A_c - 1$, respectively. For h_s, the domain G_s is twice the amplitude of the current, and the domain has positive values. However, for h_d, the amplitude domain extends from negative to positive values. In the signals, there are positive and negative values. To avoid the negative currents in h_d and to align both domains, negative currents are adjusted to the values of h_s. After that, h_s and h_d are normalized considering the number of samples in the histogram as N for obtaining the probability density function of the current, as shown in Equation (2). This equation requires that vectors S, h_s, and h_s have the same number of elements as defined in Equation (3).

$$\hat{h_s}(i) = h_s(i)/N \qquad \hat{h_d}(j) = h_d(j)/N \tag{2}$$

$$N = \sum_i h_s(i) = \sum_j h_d(j) \tag{3}$$

Summarizing, the displacements (Δ) are applied to the current signal (S), which contains N samples represented in Figure 6 according to the set of the distances defined in Δ. Each value is calculated by adding or subtracting the reference value R_s and its neighboring value Δ to compute the histograms h_s and h_d.

Using the SDH, the texture features proposed in [25] are calculated considering a predefined window size $W_s = 3$ and different displacements in Δ for better characterization of the current $S(n)$. Table 1 illustrates the nine texture features extracted, where $\hat{h}_s(i)$ is the histogram indicated by indexes $R_s \times i$ and $\hat{h}_d(j)$ is the histogram shown by indexes $R_s \times j$. Three tests were performed to validate different displacements Δ to find the predominant points in the acquired signal. Test A and Test B were the initial configurations used to evaluate the classification faults in motors. Based on these classification results, the best displacements are used to perform Test C to distinguish the most representative among the nine features. Displacements distributed between the tests are described in the following section.

Table 1. Texture features calculated from SDH [25].

Texture Feature	Definition
Mean	$\frac{1}{2}\sum_i i * \hat{h_s}(i) = \mu$
Variance	$\frac{1}{2}\{\sum_i (i-2\mu)^2 * \hat{h_s}(i) + \sum_j j^2 * \hat{h_d}(j)\}$
Energy	$\sum_i \hat{h_s}(i)^2 * \sum_j \hat{h_d}(j)^2$
Correlation	$\frac{1}{2}\{\sum_i (i-2\mu)^2 * \hat{h_s}(i) - \sum_j j^2 * \hat{h_d}(j)\}$
Entropy	$\sum_i \hat{h_s}(i) * log\{\hat{h_s}(i)\} - \sum_j \hat{h_d}(j) * log\{\hat{h_d}(j)\}$
Contrast	$\sum_j j^2 * \hat{h_d}(j)$
Homogeneity	$\sum_j \frac{1}{1+j^2} * \hat{h_d}(j)$
Cluster shade	$\sum_i (i-2\mu)^3 * \hat{h_s}(i)$
Cluster prominence	$\sum_i (i-2\mu)^4 * \hat{h_s}(i)$

2.3. Settings

As mentioned above, the displacements through the vector S for calculating the texture features in Table 1 represent the resolution of the sliding window for overlapping sampling around the reference point R_s. These displacements presented in Table 2 are the Δ values used during the SDH calculation for Tests A, B, and C.

Table 2. Proposed configurations for evaluating current characterization.

Test A	Test B	Test C
$A_1 = (-1\ 1)$	$B_1 = (-1\ 1)$	C_1 = Mean
$A_2 = (-2\ 2)$	$B_2 = (-2\ -1\ 1\ 2)$	C_2 = Variance
$A_3 = (-3\ 3)$	$B_3 = (-3\ -2\ -1\ 1\ 2\ 3)$	C_3 = Energy
$A_4 = (-4\ 4)$	$B_4 = (-\ 4\ -3\ -2\ -1\ 1\ 2\ 3\ 4)$	C_4 = Correlation
$A_5 = (-5\ 5)$	$B_5 = (-5\ -\ 4\ -3\ -2\ -1\ 1\ 2\ 3\ 4\ 5)$	C_5 = Entropy
$A_6 = (-6\ 6)$	$B_6 = (-6\ -5\ -\ 4\ -3\ -2\ -1\ 1\ 2\ 3\ 4\ 5\ 6)$	C_6 = Contrast
$A_7 = (-7\ 7)$		C_7 = Homogeneity
$A_8 = (-8\ 8)$		C_8 = Cluster shade
$A_9 = (-9\ 9)$		C_9 = Cluster prominence
$A_{10} = (-10\ 10)$		

- Test A: Test A was designed to perform incremental displacements of the Δ values in the SDH algorithm from 1 to 10. From this test, ten vectors per feature are computed, yielding 90 feature vectors in total.
- Test B: This setup performs cumulative increments in the SDH algorithm for six displacements. Then, six vectors per feature are obtained for 54.
- Test C: From the best result obtained in Test A and Test B, the displacements are used to assess the texture features. This test receives nine vectors for each computed attribute to find the best performance feature.

2.4. Classifiers

The classification stage is an instance of supervised learning that identifies the data category among several types based on a previous training stage [26,27]. The classifiers use the texture features matrix to tune the parameters. The dimensionality of data increases following the Δ values described above for Test A and Test B. Initially, a decision tree classifier is trained to detect the failure of 1BRB, 2BRB, and Health from the acquired signals S. This classifier is used due to its straightforward calculation methodology, making it computationally efficient. Likewise, it provides a good result in terms of precision and accuracy by determining the texture feature with the highest gain within the analyzed dataset [28]. Based on the results of Test C, two more classifiers were trained, the bagged decision tree and the k-nearest neighbor classifier. The main objective of the multi-classifier analysis is to improve accuracy because, in the case of biased data, the learning stage of

a decision tree may also be biased. The bagged decision tree algorithm builds multiple tree-like structures trained with a random selection of subsets to make classifications. This process is performed repeatedly by replacing the trees and training each weak algorithm with the selected subsets [29]. The classification algorithms are tested using Matlab's corresponding machine learning and statistics toolbox functions.

3. Results

This section evaluates the proposed classification method to analyze the displacement configuration and texture that obtains the best performance. The analysis of a single-phase current in induction motors evaluates two sets of different Δ displacements defined in Tests A and B. Moreover, the experiments are conducted using a fixed value for the analysis window W_s, nine texture features, and comparing the accuracy performance of three classifiers.

To perform the tests, 30 current signals for each category were analyzed from an induction motor diagnosed with 1BRB, 2BRB, and Health. From these signals, 153 histograms were obtained, divided as follows: for Test A 90 vectors, for Test B 54 vectors, and nine for Test C. Table 3 shows the accuracy classification results obtained by a multiclass decision tree for the three tests performed. Decision trees offer all the advantages of any other more robust classifier. However, the disadvantages of this classifier can be reduced by compensating hyperparameters required for determining the best configuration to train the model [30]. Therefore, the complexity of training a decision tree is controlled by the parameter that governs the process. Table 4, and Figure 7a specifies the tuning parameters evaluated in each iteration to achieve the best performance. Furthermore, Table 5 shows the summary of the decision tree tuning parameters with the best performance, and Figure 7b shows the estimated objective function value.

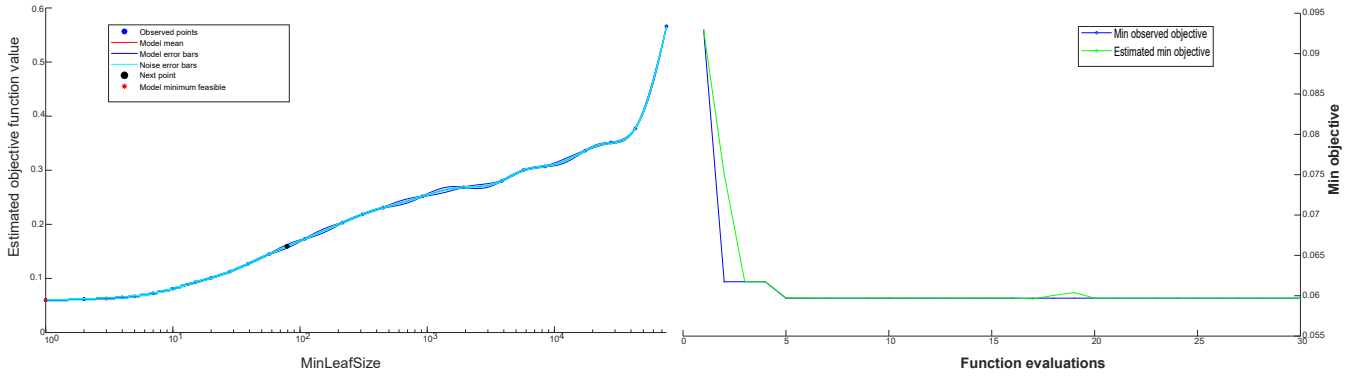

(**a**) (**b**)

Figure 7. Hyperparameter optimization performance graphs. (**a**) Objective function model. (**b**) Min objective vs. function evaluations.

Table 3. The accurate results for the performed tests for decision tree classifier.

Test A		Test B		Test C	
A_1	81.76%	B_1	81.76%	C_1	42.8%
A_2	80.12%	B_2	81.66%	C_2	40.51%
A_3	79.92%	B_3	83.16%	C_3	88.20%
A_4	84.79%	B_4	87.93%	C_4	59.95%
A_5	83.84%	B_5	91.40%	C_5	86.53%
A_6	84.23%	B_6	93.37%	C_6	68.63%
A_7	87.23%			C_7	98.05%
A_8	90.07%			C_8	46.30%
A_9	87.17%			C_9	58.75%
A_{10}	85.94%				

Table 4. Hyperparameters (decision trees) for Test C_7.

Iteration	Best Observed	Best Estimated	Iteration	Best Observed	Best Estimated
1	0.377380	0.377380	16	0.058669	0.058932
2	0.254860	0.266290	17	0.058669	0.058645
3	0.137740	0.137790	18	0.058669	0.058685
4	0.065611	0.065584	19	0.058669	0.058689
5	0.058669	0.058120	20	0.058669	0.058773
6	0.058669	0.059034	21	0.058669	0.058808
7	0.058669	0.058826	22	0.058669	0.058937
8	0.058669	0.058769	23	0.058669	0.058980
9	0.058669	0.058740	24	0.058669	0.059034
10	0.058669	0.058748	25	0.058669	0.059115
11	0.058669	0.587110	26	0.058669	0.058672
12	0.058669	0.058711	27	0.058669	0.058672
13	0.058669	0.058715	28	0.058669	0.058672
14	0.058669	0.558560	29	0.058669	0.058672
15	0.058669	0.057117	30	0.058669	0.058672

Table 5. Best configuration for Test C_7.

Best Observed Feasible Point	
Observed objective function value	0.058669
Estimated objective function value	0.058672
Evaluation time	11.3949 (s)

From the total samples in the dataset, 75% were selected for training and 25% were selected for validation. Thirty tests were performed, choosing the above percentage; however, the examples were randomly selected for training and validation during the experimental tests. Based on these results of Tests A and B, the best Δ displacements are B_6, which are used to perform the analysis in Test C. Notably, the best percentage in Test C among all the analyzed features is C_7, corresponding to the homogeneity attribute. Test C's classification accuracy is above 80% for three texture attributes. These results show that the proposed methodology is reliable as multiple texture features can characterize the method. Furthermore, we can consider adding signals from other motor states to be analyzed for increasing the number of faults. Therefore, additional analysis using the homogeneity feature is performed using a polynomial regression curve. This analysis validates the performance of classification as the number of samples increases. The processing time of texture features depends on the number of displacements performed. We have proposed three displacement sets; therefore, the processing time differs. In this case, the processing time for feature extraction, training, and validation of the analyzed signal is shown in Table 6.

Table 6. Process computational time for C_7.

Process	Time	σ
Feature extraction	296.20 ms	16.10 ms
Training	15.50 s	1.97 s
Validation	18.35 µs	48.52 µs

According to the confusion matrix shown in Figure 8a, the motor state that provides the best classification result is one broken rotor bar. Moreover, Figure 8b shows the analysis history from the initial samples evaluated through a polynomial regression curve. Based on this plot, it can be noticed that the processing of 50 samples obtains an acceptable result,

with an accuracy of 88.15%. At the end of the plot, it can be shown that 250 samples obtain an accuracy of 98.05%.

Considering the percentage results obtained from the polynomial regression curve, additional classification tests were performed. At this stage of the experimental tests, the B_6 displacements resulting from Test B and the best feature in Test C were considered. The accuracy percentages per class are shown in Figure 9 and have been obtained using the homogeneity texture for two different classifiers. The classification accuracy achieved is 98.16% using the Bagged decision tree and 91.4% for K-NN.

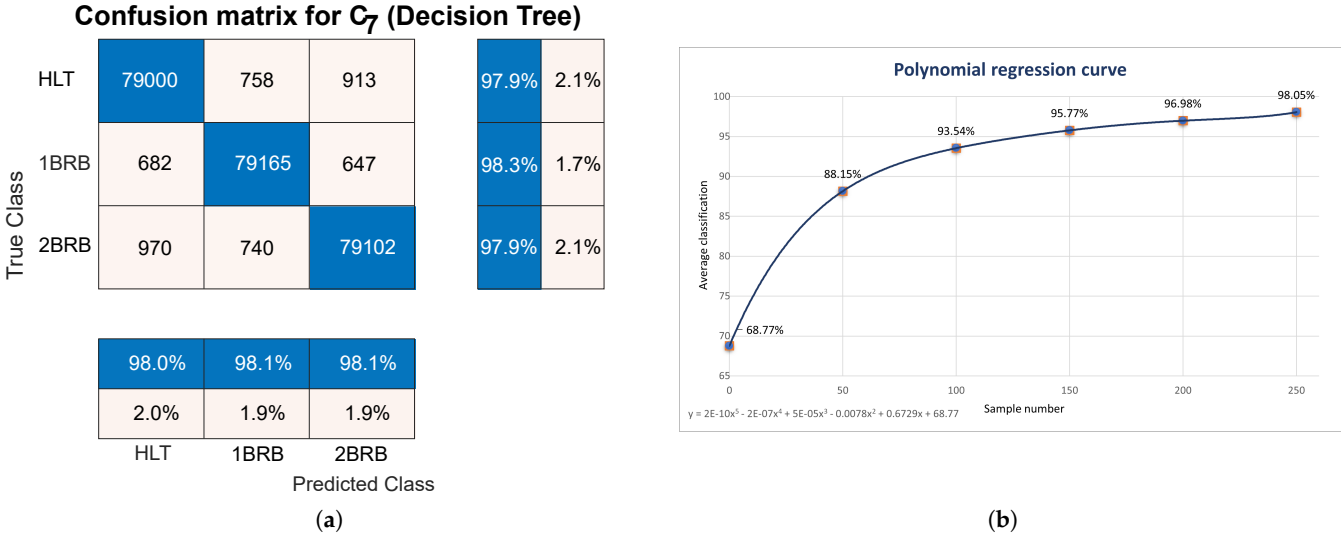

(**a**) (**b**)

Figure 8. Classification results for the homogeneity texture (C_7) of Table 3. (**a**) Confusion matrix for C_7. (**b**) Polynomial regression curve for decision tree.

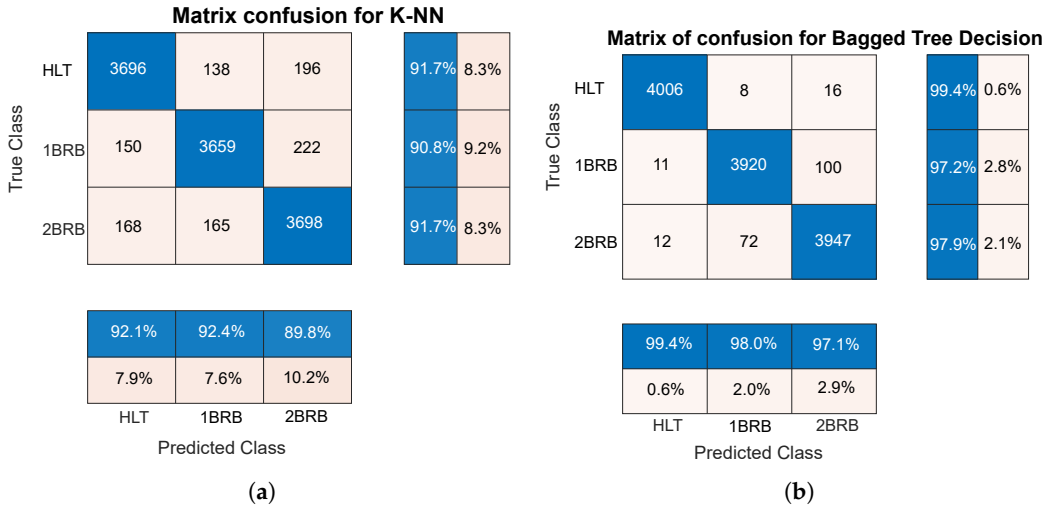

(**a**) (**b**)

Figure 9. Confusion matrices obtained for homogeneity feature. (**a**) K-nearest neighbor. (**b**) Bagged decision tree.

Table 7 compares the proposed approach with previous works in the literature. The second column in the table presents the methods, the third column the type of faults, the fourth column the type of signal, the fifth the domain of analysis, and finally, the accuracy. The proposed method achieves an accuracy of 98.16% using fundamental and low-complexity arithmetic operations. The nature of the proposed algorithm allows for parallelization of the computations to speed up the processing. However, authors in [31] achieved a 100% accuracy in induction motor classification of HLT, 1BRB, and 2BRB. This processing implies filtering the signal to perform convolutional processing, demanding high

computational resources. The accuracy difference is irrelevant to our proposed conventional computational resource approach.

Likewise, in [22], the authors initially filtered the signal; then, an analysis window was used for segmenting and detecting BRB under different motor loads. The final detection consisted of checking the presence of BRB without considering additional motor conditions and achieving a lower percentage than the proposed method. On the other hand, in [32], the authors presented a dataset obtained through an Ansys Maxwell simulator to generate synthesized signals for evaluating the signal decomposition with cross-correlation. The results are promising; however, simulated signals do not provide real motor behavior. In [33], authors developed a similar methodology to our approach for detecting HLT, 1BRB, and 2BRB, obtaining an accuracy of 98.3%. However, our system proposes a more robust analysis that includes nine texture features for describing motor behavior.

Table 7. Comparison with related works.

Work	Methodology	Fault	Signal Type	Domain	Accuracy
Valtierra et al. [31]	1. Fourier transform 2. CNN as estimator and classifier	HBRB 1BRB 2BRB	Current	Time Frequency	100%
Cleber et al. [22]	1. Histogram of Oriented Gradients 2. Bayesian classifier.	BRB	Current	Time	96%
Yang et al. [32]	1. MEEMD energy entropy 2. Artificial neural network	BRB	Current	Time	99%
Ferrucho et al. [33]	1. Contrast calculation 2. Fuzzy logic	1BRB 2BRB	Current	Time	98.3%
Our approach	1. SDH. 2. Texture features.	HLT 1BRB 2BRB	Current	Time	98.16%

4. Conclusions

In this work, we proposed the detection of 1BRB and 2BRB faults in induction motors by applying statistical analysis of one phase's electrical current in the time domain. The main contribution is to provide a low-complexity method combining local statistical methods and standard machine learning classifiers that could be quickly and easily embedded for real-time fault detection. The analysis of nine texture characteristics with different displacements demonstrates the careful comparison of the current behavior varying the sampling points and, consequently, the resolution of the features. The three tests performed help to find the most relevant feature and distances, obtaining 98.16% of global performance for three motor condition classifications using a bagged decision Tree. Moreover, regression analysis shows that our method obtained an acceptable accuracy of 88.15% using only 50 samples but also achieved a percentage of 98.05% for 250 samples, reducing the amount of data to process. Compared to related works, our method shows high classification results using electrical current acquired from an induction motor, avoiding high-computational-cost classifiers and optimizing the number of samples.

This method could include additional motor faults that the proposed multi-displacement analysis of textures can easily characterize. As a future work, this method could include multiple motor faults by considering three-phase current signals to detect short circuits in the motor coils and impedance estimation by analyzing the offset between voltage and current signals.

Author Contributions: Conceptualization, D.-L.A.-O. and M.-A.I.-M.; Methodology, V.H.-R. and M.-A.I.-M.; Software, V.H.-R.; Validation, J.-L.C.-H. and M.-A.I.-M.; Formal analysis, V.H.-R., D.-L.A.-O. and M.-A.I.-M.; Investigation, J.-J.C.-C.; Resources, J.-L.C.-H.; Data curation, V.H.-R.; Writing—original draft, V.H.-R.; Writing—review & editing, D.-L.A.-O., J.-J.C.-C. and J.-L.C.-H.; Visualization, D.-L.A.-O.; Supervision, D.-L.A.-O. and M.-A.I.-M. All authors have read and agreed to the published version of the manuscript.

Funding: This research was funded by CONAHCyT grants 738317 and 809170. Universidad de Guanajuato funded the APC under POA 2023.

Institutional Review Board Statement: Not applicable.

Informed Consent Statement: Not applicable.

Data Availability Statement: Motor signals database and their corresponding diagnosis were provided in collaboration with national and international partners based on a privacy agreement with the University of Guanajuato. The agreement avoids publicly sharing or distributing any kind of data.

Conflicts of Interest: The authors declare no conflict of interest. Also, the funders had no role in the study's design, in the collection, analysis, or interpretation of data, in the writing of the manuscript, or in the decision to publish the results.

References

1. Gangsar, P.; Tiwari, R. Signal based condition monitoring techniques for fault detection and diagnosis of induction motors: A state-of-the-art review. *Mech. Syst. Signal Process.* **2020**, *144*, 106908. [CrossRef]
2. Almounajjed, A.; Sahoo, A.K.; Kumar, M.K. Diagnosis of stator fault severity in induction motor based on discrete wavelet analysis. *Measurement* **2021**, *182*, 109780. [CrossRef]
3. Zamudio-Ramírez, I.; Ramirez-Núñez, J.; Antonino-Daviu, J.; Osornio-Rios, R.; Quijano-Lopez, A.; Razik, H.; Jesus Romero-Troncoso, R. Automatic Diagnosis of Electromechanical Faults in Induction Motors Based on the Transient Analysis of the Stray Flux via MUSIC Methods. *IEEE Trans. Ind. Appl.* **2020**, *56*, 3604–3613. [CrossRef]
4. Saucedo-Dorantes, J.; Delgado-Prieto, M.; Romero-Troncoso, R.; Osornio-Rios, R. Multiple-fault detection and identification scheme based on hierarchical self-organizing maps applied to an electric machine. *Appl. Soft Comput.* **2019**, *81*, 105497. [CrossRef]
5. Contreras-Hernandez, J.; Almanza-Ojeda, D.; Ledesma, S.; Garcia-Perez, A.; Castro-Sanchez, R.; Gomez-Martinez, M.; Ibarra-Manzano, M. Geometric Analysis of Signals for Inference of Multiple Faults in Induction Motors. *Sensors* **2022**, *22*, 2622. [CrossRef]
6. Saucedo-Dorantes, J.; Zamudio-Ramirez, I.; Cureno-Osornio, J.; Osornio-Rios, R.; Antonino-Daviu, J. Condition Monitoring Method for the Detection of Fault Graduality in Outer Race Bearing Based on Vibration-Current Fusion, Statistical Features and Neural Network. *Appl. Sci.* **2021**, *11*, 8033. [CrossRef]
7. Kumar, P.; Hati, A. Deep convolutional neural network based on adaptive gradient optimizer for fault detection in SCIM. *ISA Trans.* **2021**, *111*, 350–359. [CrossRef]
8. Gangsar, P.; Tiwari, R. A support vector machine based fault diagnostics of Induction motors for practical situation of multi-sensor limited data case. *Measurement* **2019**, *135*, 694–711. [CrossRef]
9. Yakhni, M.; Cauet, S.; Sakout, A.; Assoum, H.; Etien, E.; Rambault, L. El-Gohary, M. Variable speed induction motors' fault detection based on transient motor current signatures analysis: A review. *Mech. Syst. Signal Process.* **2023**, *184*, 109737. [CrossRef]
10. Esakimuthu Pandarakone, S.; Mizuno, Y.; Nakamura, H. A Comparative Study between Machine Learning Algorithm and Artificial Intelligence Neural Network in Detecting Minor Bearing Fault of Induction Motors. *Energies* **2019**, *12*, 2105. [CrossRef]
11. Ameid, T.; Menacer, A.; Talhaoui, H.; Azzoug, Y. Discrete wavelet transform and energy eigen value for rotor bars fault detection in variable speed field-oriented control of induction motor drive. *ISA Trans.* **2018**, *79*, 217–231. [CrossRef] [PubMed]
12. Senthil Kumar, R.; Gerald Christopher Raj, I.; Alhamrouni, I.; Saravanan, S.; Prabaharan, N.; Ishwarya, R.; Gokdag, M.; Salem, M. A combined HT and ANN-based early broken bar fault diagnosis approach for IFOC fed induction motor drive. *Alex. Eng. J.* **2023**, *66*, 15–30. [CrossRef]
13. Siddiqui, K.M.; Mohan, M. Modelling and detection and of rotor and broken bar and fault using and induction motor and fed pwm and inverter. *J. Comput. Sci. Technol.* **2012**, *7*, 353–358.
14. Godoy, W.F.; da Silva, I.N.; Goedtel, A.; Palacios, R.H.C.; Lopes, T.D. Application of intelligent tools to detect and classify broken rotor bars in three-phase induction motors fed by an inverter. *IET Electr. Power Appl.* 2016, *10*, 430–439. [CrossRef]
15. Nuzzo, R. Histograms: A Useful Data Analysis Visualization. *PM R* **2019**, *11*, 309–312. [CrossRef]
16. Khamisan, N.; Ghazali, K.H.; Almisreb, A.; Muhammad Zin, A.H. Histogram-based of Healthy and Unhealthy Bearing Monitoring in Induction Motor by Using Thermal Camera. *J. Telecommun. Electron. Comput. Eng. (JTEC)* **2018**, *10*, 31–35.
17. Al-Musawi, A.; Anayi, F.; Packianather, M. Three-phase induction motor fault detection based on thermal image segmentation. *Infrared Phys. Technol.* **2020**, *104*, 103140. [CrossRef]

18. Resendiz-Ochoa, E.; Osornio-Rios, R.; Benitez-Rangel, J.; Romero-Troncoso, R.J.; Morales-Hernandez, L. Induction Motor Failure Analysis: An Automatic Methodology Based on Infrared Imaging. *IEEE Access* **2018**, *6*, 76993–77003. [CrossRef]
19. Yaman, O. An automated faults classification method based on binary pattern and neighborhood component analysis using induction motor. *Measurement* **2021**, *168*, 108323. [CrossRef]
20. Lopez-Ramirez, M.; Ledesma-Carrillo, L.; Garcia-Guevara, F.; Munoz-Minjares, J.; Cabal-Yepez, E.; Villalobos-Pina, F. Automatic Early Broken-Rotor-Bar Detection and Classification Using Otsu Segmentation. *IEEE Access* **2020**, *8*, 112624–112632. [CrossRef]
21. Kerboua, A.; Metatla, A.; Kelailia, R.; Batouche, M. Fault Diagnosis in Induction Motor using Pattern Recognition and Neural Networks. In Proceedings of the 2018 International Conference On Signal, Image, Vision And Their Applications (SIVA), Guelma, Algeria, 26–27 November 2018; pp. 1–7.
22. Dias, C.G.; da Silva, L.C.; Alves, W.A.L. A Histogram of Oriented Gradients Approach for Detecting Broken Bars in Squirrel-Cage Induction Motors. *IEEE Trans. Instrum. Meas.* **2020**, *69*, 6968–6981. [CrossRef]
23. Say, M. *The Performance and Design of Alternating Current Machines*; CBS Publisher Distributors, Illustrated: New Delhi, India, 2005.
24. Subrata, K.; Surajit, C.; Madhuchh, A.M.; Samarjit, S. *Induction Motor Fault Diagnosis Approach through Current Signature Analysis*; Springer: Singapore, 2016.
25. Unser, M. Sum and difference histograms for texture classification. *IEEE Trans. Pattern Anal. Mach. Intell.* **1986**, *1*, 118–125. [CrossRef] [PubMed]
26. Belguesmi, L.; Hajji, M.; Mansouri, M.; Harkat, M.-F.; Kouadri, A.; Nounou, H.; Nounou, M. Machine learning approaches for fault detection and diagnosis of induction motors. In Proceedings of the 2020 17th International Multi-Conference on Systems, Signals & Devices, Monastir, Tunisia, 20–23 July 2020.
27. Bazan, G.H.; Goedtel, A.; Scalassara, P.R.; Endo, W.; Nunes, E.A.; Takase, V.T.F.; Guedes, J.J.; Gentil, M.G. An embedded system for stator short-circuit diagnosis in three-phase induction motors using information theory and artificial neural networks. *IEEE Trans. Syst. Man Cybern. Syst.* **2022**, *52*, 6582–6592. [CrossRef]
28. Patange, A.D.; Jegadeeshwaran, R. A machine learning approach for vibration-based multipoint tool insert health prediction on vertical machining centre (VMC). *Measurement* **2021**, *173*, 108649. [CrossRef]
29. Khade, H.S.; Patange, A.D.; Pardeshi, S.S.; Jegadeeshwaran, R. Design of bagged tree ensemble for carbide coated inserts fault diagnosis. *Mater. Today Proc.* **2021**, *46*, 1283–1289. [CrossRef]
30. Patange, A.D.; Pardeshi, S.S.; Jegadeeshwaran, R.; Zarkar, A.; Verma, K. Augmentation of decision tree model through hyper-parameters tuning for monitoring of cutting tool faults based on vibration signatures. *J. Vib. Eng. Technol.* **2022**, 1–19. [CrossRef]
31. Valtierra-Rodriguez, M.; Rivera-Guillen, J.R.; Basurto-Hurtado, J.A.; De-Santiago-Perez, J.J.; Granados-Lieberman, D.; Amezquita-Sanchez, J.P. Convolutional Neural Network and Motor Current Signature Analysis during the Transient State for Detection of Broken Rotor Bars in Induction Motors. *Sensors* **2020**, *20*, 3721. [CrossRef]
32. Yang, Z.; Kong, C.; Wang, Y.; Rong, X.; Wei, L. Fault diagnosis of mine asynchronous motor based on MEEMD energy entropy and ANN. *Comput. Electr. Eng.* **2021**, *92*, 107070. [CrossRef]
33. Ferrucho-Alvarez, E.R.; Martinez-Herrera, A.L.; Cabal-Yepez, E.; Rodriguez-Donate, C.; Lopez-Ramirez, M.; Mata-Chavez, R.I. Broken Rotor Bar Detection in Induction Motors through Contrast Estimation. *Sensors* **2021**, *21*, 7446. [CrossRef]